Heliyon 9 (2023) e22656

Contents lists available at ScienceDirect

Heliyon

journal homepage: www.cell.com/heliyon

Comprehensive analysis of single-cell and bulk RNA-sequencing data identifies B cell marker genes signature that predicts prognosis and analysis of immune checkpoints expression in head and neck squamous cell carcinoma

Dilinaer Wusiman [a], Wenbin Li [b], Lei Guo [b], Zehao Huang [a], Yi Zhang [b], Xiwei Zhang [a], Xiaohui Zhao [a], Lin Li [b], Zhaohong An [a], Zhengjiang Li [a,***], Jianming Ying [b,**], Changming An [a,*]

[a] *Department of Head and Neck Surgery, National Cancer Center, National Clinical Research Center for Cancer, Cancer Hospital, Chinese Academy of Medical Sciences and Peking Union Medical College, Beijing, 100021, China*

[b] *Department of Pathology, National Cancer Center, National Clinical Research Center for Cancer, Cancer Hospital, Chinese Academy of Medical Sciences and Peking Union Medical College, Beijing, 100021, China*

ARTICLE INFO

Keywords:
Head and neck squamous cell carcinoma
B cell marker genes
Prognosis
Immune checkpoints
Immunohistochemistry

ABSTRACT

Recent studies have shown that B cells and the associated tertiary lymphoid structures (TLS) correlate with the response of patients to immune checkpoint inhibitors (ICIs) and predict overall survival (OS) in cancer patients. We screened 145 B cell marker genes (BCMG) by a comprehensive analysis of single-cell RNA-sequencing (scRNA-seq) data of head and neck squamous cell carcinoma (HNSC) from the Gene Expression Omnibus (GEO) database. The BCMG signature (BCMGS) was established using The Cancer Genome Atlas (TCGA) dataset of HNSC and verified in four independent datasets. The multivariate Cox regression analysis identified the signature as an independent prognostic factor. A prognostic nomogram was constructed with independent prognostic factors using the TCGA dataset. GO and KEGG analysis revealed the underlying signaling pathways related to this signature. Study of immune profiles showed that patients in the low-risk group presented discriminative immune-cell infiltrations. Furthermore, the low-risk group was featured by higher TCR and BCR diversity, which suggested that low-risk patients may be more sensitive to ICIs. Immunohistochemistry was performed, and we found that high expression of FTH1 was significantly correlated with poor OS ($P = 0.025$). The expression of TIM-3, LAG-3 and PD-1 was positively correlated and associated with better OS in HNSC. However, there was no statistically significant difference between PD-L1, PD-L2, CTLA-4, TIGIT and prognosis. The BCMGS was a promising prognostic biomarker in HNSC, which may help to interpret the responses to immunotherapy and provide a new perspective for future research on the treatment in HNSC.

* Corresponding author.
** Corresponding author.
*** Corresponding author.
E-mail addresses: lizhengjiang@cicams.ac.cn (Z. Li), jmying@cicams.ac.cn (J. Ying), anchangming@cicams.ac.cn (C. An).

https://doi.org/10.1016/j.heliyon.2023.e22656
Received 20 June 2023; Received in revised form 13 November 2023; Accepted 16 November 2023
Available online 24 November 2023

1. Introduction

Head and neck cancer is the eighth most frequent type of tumor worldwide in the report of GLOBOCAN 2020 [1], and squamous cell carcinoma accounts for over 90 % of head and neck cancer [2]. Head and neck squamous cell carcinoma (HNSC) arises from these five major anatomical sites: the oral cavity, oropharynx, hypopharynx and nasopharynx, and larynx [3]. In addition to smoking and chronic heavy alcohol consumption [4,5], human papillomaviruses (HPV) infection is another independent risk factor of HNSC globally [6], especially in oropharyngeal cancers [7]. In recent years, the implementation of immune checkpoint inhibition (ICI) has substantially improved therapeutic outcomes for relapsed or metastatic HNSC patients. KEYNOTE-048 study, the landmark phase III clinical trial, demonstrated that pembrolizumab plus chemotherapy significantly improved overall survival (OS) compared with cetuximab plus chemotherapy in patients with advanced or metastatic HNSC [8]. Although many patients with HNSC benefits from immunotherapy significantly, there are still many patients who do not benefit from immunotherapy or even suffer from life-threatening immunotoxicities [9]. Thus, it is essential to develop an effective biomarker to predict immunotherapy response.

Two RNA-seq methods are now commonly considered in tumor immunology research: standard bulk RNA-seq and single-cell RNA-seq (scRNA-seq). Bulk RNA-seq is widely used in many fields of tumor, especially in the discovery of cancer biomarkers for disease diagnosis and prognosis prediction, etc. Measurements of standard bulk RNA-seq data are summed over populations of different cell types in a tissue, thus ignoring the heterogeneity of individual cells. Single-cell RNA-sequencing (scRNA-seq) is a powerful deep molecular profiling method for detecting different cell types, states, and functions in cancer [10]. ScRNA-seq allows researchers to dissect this heterogeneity and identify specific cell types, including B cells, and their gene expression profiles. By integrating single cell and bulk RNA-seq data, we could obtain reliable estimation of cell type specific gene expression profiles [11].

Infiltration of the immune system into the tumor microenvironment (TME) has been shown to play a critical role in tumor

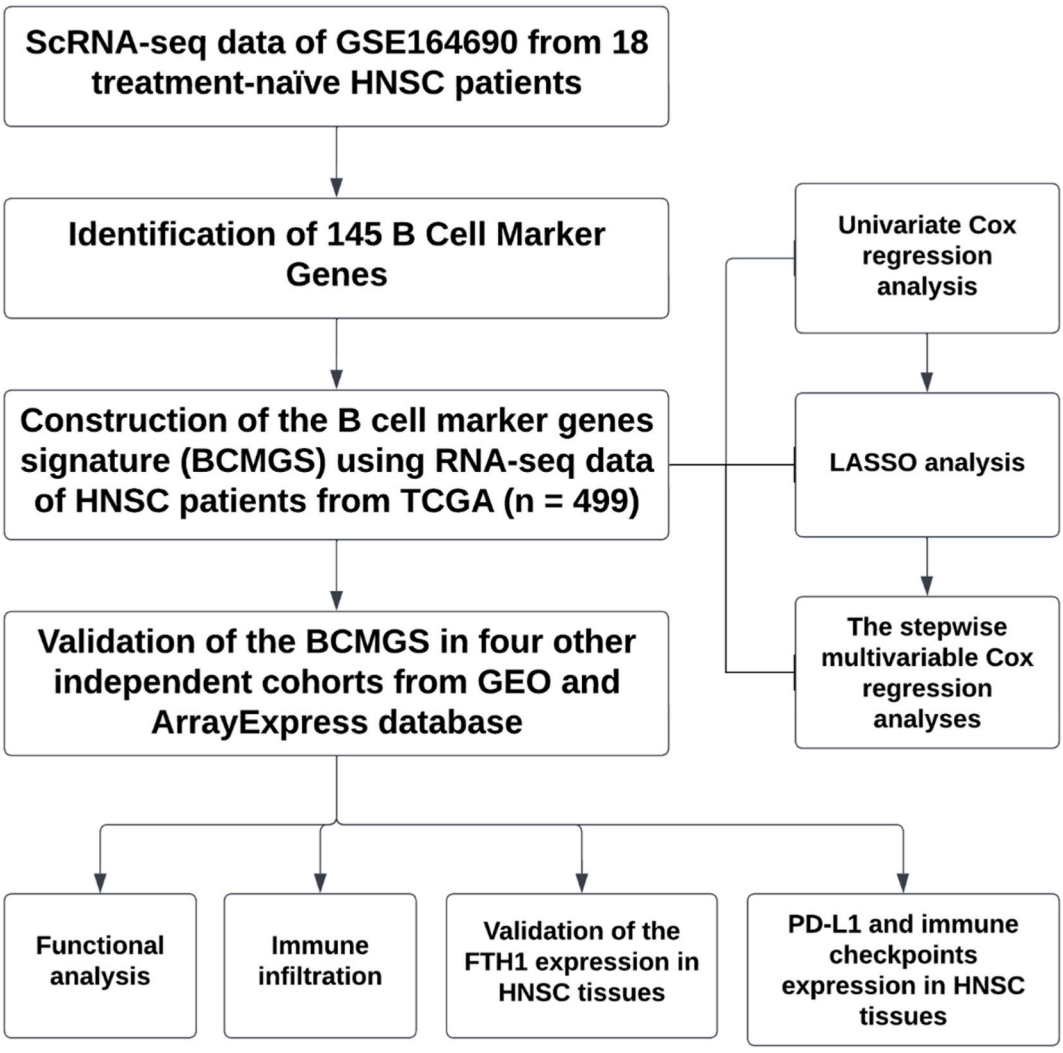

Fig. 1. Overall flowchart of patients' enrollment and data processing.

development and influence clinical outcomes in cancer patients. B cells and T cells play a crucial role in cell-mediated immune responses and humoral immune responses [12,13]. However, the heterogeneity and dynamics of the TME hinder the precise dissection of immune cells within tumors. Recent advances in single-cell RNA sequencing (scRNA-seq) allow systematic TME testing and bring important insights into tumor-infiltrating lymphocytes (TILs) [14]. Cancer immunology continues to focus on T cells, but a recent series of articles agree that B cell infiltration in human cancers is associated with better T cell responses [15]. And the activated B cells in tertiary lymphoid structures (TLS) were associated with improved clinical outcomes and improved immunotherapy response to several cancer types [16–19]. Gene expression signatures showed their utility as a biomarker of ICIs, and relative research is currently one of the hot spots in immunotherapy biomarker research. Several immune checkpoints (ICs) control T cell-mediated cytotoxic reactions, which also encourage people to employ immune checkpoint inhibitors for combination therapy. The suppressor FTH1 is independent prognostic factor and independently correlated with M1 and M2 macrophage infiltration in HNSC [20]. FTH1 also plays an important role in regulating tumor immunity to solid cancers [21], which made us interested in the specific regulatory mechanism of FTH1.

Up to now, there is still a lack of research using the expression of B cell marker genes to develop molecular biomarkers and prognostic signatures for HNSC. In the present study, we firstly screened B cell marker genes of HNSC using single-cell RNA sequencing (scRNA-seq) data from the GEO database. Then, RNA sequencing (RNA-seq) data from TCGA and four independent datasets were used to develop and validate a prognostic model of B cell marker genes. Furthermore, we used the independent risk factors obtained by multivariate Cox regression analysis to construct a nomogram of OS to increase the accuracy of prognosis prediction for HNSC patients. We explored the relationship between the signature and some indicators for immunotherapy response, such as the landscape of immune cell infiltration, TCR diversity, and BCR diversity, to explore the potential role of the signature in identifying the response to immunotherapy. We revealed the clinicopathological implications of the FTH1, PD-L1, PD-L2, PD-1, TIM-3, LAG-3, CTLA-4, and TIGIT using immunohistochemistry (IHC). The overall flowchart was showed in Fig. 1.

2. Materials and methods

2.1. Data sources

The Cancer Genome Atlas (TCGA) level three RNA-seq data of 499 HNSC samples (Illumina HiSeq 2000) with OS information was acquired from the Cancer Genomics Browser of the University of California Santa Cruz (UCSC) [22] (http://xena.ucsc.edu/). And we also collected the corresponding clinical data and mutation data of these 499 patients from UCSC. Then we converted the FPKM value to the TPM value, which was more similar to those results from microarrays and more comparable between samples [23]. Three Gene Expression Omnibus (GEO) datasets with clinical annotations and OS information were obtained from the GEO database (https://www.ncbi.nlm.nih.gov/geo/) and one from ArrayExpress database (https://www.ebi.ac.uk/arrayexpress/). The GSE41613 [24], GSE42743 [24], GSE65858 [24] and E-MTAB-8588 [25] expression profile respectively contained 97, 74, 270 and 108 HNSC samples. We obtained the Single-cell RNA sequencing data from 18 treatment naïve HNSC samples of GSE164690 [26] from the GEO database, and the B cell marker genes of HNSC were analyzed from it. The patients from TCGA were defined as the training set, while the four datasets from the GEO and ArrayExpress database were used for external validation. In addition, the detailed clinical information of TCGA and GEO datasets was collected, including age, sex, grades, TNM stage, and OS status.

2.2. Identification of B cell marker genes by scRNA-seq analysis

We implemented the quality control measure to ensure the high quality of cells remained and removed cells with >5000 genes, <200 genes, or >10 % mitochondrial counts. We first created a Seurat object for each sample and put it in the scRNA list. Each matrix was transformed by the "LogNormalize" method of the "NormalizeData" function, and the "vst" method of the "FindVariableFeatures" function was used to identify the top 2000 highly variable genes. Normalized scRNA-seq data of each sample were combined as a Seurat object with the "FindVariableFeatures" and "IntegrateData" functions. ScaleData function and RunPCA function were used for principal component analysis (PCA) for the 2000 highly variable genes, and the first 15 principal components (PCs) were used for t-SNE. Then we divided the cell types, including T cells, B cells, Monocyte, NK cells and epithelial cells. Each cell cluster was annotated with the Human Primary Cell Atlas [27]. And linked the marker genes from each cluster to the appropriate cell types. Cell clustering analysis was performed using the "FindNeighbors" and "FindClusters" functions (the clustering resolution = 0.5) in the "Seurat" package. And FindAllMarkers functions were used to cluster cells and identify the differentially expressed genes (DEGs) of each cluster with the cut-off of adjusted p-value <0.01 and logFC.threshold = log2(2).

2.3. Construction and verification of a prognostic model based on B cell marker genes

The prognostic model was constructed based on the TCGA dataset, which was set as the training cohort. Each gene among the expression profiles was normalized using log2 transformation. The univariate Cox proportional hazard regression analysis was used to screen B cell marker genes which were related to survival ($P < 0.05$). The least absolute shrinkage and selection operator (LASSO) regression was performed using the R package "glmnet" (version 4.1–3) to minimize the risk of overfitting [28]. Then, the stepwise multivariate Cox proportional hazards regression model was used to identify the most relevant genes associated with survival and to construct a prediction model based on these B cell marker genes. The expression (exp) of these B cell marker genes and the regression coefficient (coef) value were used to calculate the risk score: Risk score = (exp(gene1) *coef(gene1) + exp(gene2) *coef(gene2) + exp

(gene3) *coef(gene3) + exp(gene4) *coef(gene4) + exp(gene5) *coef(gene5)). High- and low-risk groups were divided according to the median risk score. The samples from three GEO datasets and one ArrayExpress database were used to validate the prediction performance of the constructed prognostic model. The Kaplan-Meier survival analysis was performed to assess the difference in OS between high- and low-risk groups. 2-, 3-, and 5-year time-dependent receiver operating characteristic (ROC) curves were depicted to assess the performance of the risk model. We conducted the prognostic meta-analysis to assess the prognostic significance of the B cell marker genes signature in different cohorts by "meta" R package (version 5.2–0).

2.4. Construction and assessment of the nomogram based on the prognostic model

A nomogram for the 2-, 3-, and 5-year OS was constructed based on the independent factors obtained by using multivariate Cox regression analysis. The discrimination of the nomogram was measured by the C-index, ROC curves, and calibration plots.

2.5. Pathway and functional enrichment analysis

DEGs between high- and low-risk groups were identified using the "limma" package in R with the cut-off of $P < 0.05$ and $|\log2$ (fold change)$| > 1$. Kyoto Encyclopedia of Genes and Genomes (KEGG) and Gene Ontology (GO) functional enrichment analysis of the BCMGS was performed. R packages were used to analyze, including "clusterProfiler" (version 4.1.5), "org.Hs.eg.db" (version 3.12.2), "enrichplot" (version 1.12.3), "ggplot2" (version 3.3.5).

2.6. Immune score, stromal score, and ESTIMATE score of high- and low-risk groups

In addition, we analyzed the relationship between risk score and tumor microenvironment by The Estimation of Stromal and Immune cells in Malignant Tumor tissues using the Expression data (ESTIMATE) algorithm, which was used to calculate the stromal score, immune score, ESTIMATE score, and tumor purity of high- and low-risk groups based on gene expression data [29]. The score of each sample was calculated using the "estimate" R package (version 1.0.13), and the difference in immune cell infiltration between high- and low-risk groups was further compared by the Wilcoxon test.

2.7. Analysis of the tumor-infiltrating immune cell

We estimated the abundance of immune cell infiltration in high- and low-risk groups in this study by the CIBERSORT algorithm, which was a novel tool that used RNA-sequencing data to evaluate the cell composition in tumors and the infiltration of immune cells [30]. The LM22 algorithm was used to conduct CIBERSORT, which contains 547 genes downloaded from the web portal (http://cibersort.stanford.edu/) that could identify 22 immune cell subtypes. We used Wilcoxon tests to analyze and the "vioplot" package (version 0.3.7) to visualize the data. We also investigated the association between the expression of 35 immune checkpoints and two risk groups.

2.8. Analysis of T cell receptor (TCR) and B cell receptor (BCR) repertoire

Diversity scores of TCR and BCR, including richness measure the number of different T-cell clones with unique TCRs and BCRs in the sample, and Shannon Entropy that access the clonotype frequencies. Based on a previous study comprising diverse cancer types, we collated the richness and Shannon diversity valves of TCR and BCR of HNSC patients from TCGA [31].

2.9. Gene expression analysis using GEPIA2

We analyzed the expression difference between the tumor tissues from TCGA and the matched normal tissues, which are from TCGA normal and GTEx (Genotype-tissue expression) data using the "Expression analysis" module of the GEPIA2 (http://gepia2.cancer-pku.cn/#analysis) with the $|\text{Log}_2\text{FC}|$ cut-off of 1 and a p-value cut-off of 0.01.

2.10. Immunohistochemistry

IHC staining was used in samples with primary HNSC and without other primary tumors. 114 cases of HNSC tissues were obtained from the Cancer Hospital, Chinese Academy of Medical Science, Beijing, China, between January 2016 and December 2017. We construct the tissue microarrays (TMAs) with formalin-fixed paraffin-embedded (FFPE) specimens using a manual tissue arrayer (Beecher Instruments Inc, Sun Prairie, WI, USA). We performed IHC staining in an automated system on the Ventana BenchMark platform (Ventana Medical Systems, Tucson, AZ). IHC staining was performed for the protein encoded by signature genes and some immune checkpoints, including FTH1, PD-L1, PD-L2, PD-1, TIM-3, LAG-3, CTLA-4, and TIGIT. Primary antibodies were purchased from Abcam (Cambridge, UK) including anti-Ferritin antibody (ab287968, 1:100 dilutions), anti-GITR antibody (ab223841, 1:1000 dilutions). T Cell Exhaustion Marker (PD-1, CTLA-4, TIM-3, LAG-3, TIGIT) Antibody Panel (ab254018, Abcam) was used, including mouse monoclonal [NAT105] to PD-1 (ab52587, 1:50 dilutions), rabbit monoclonal [CAL49] to CTLA-4 (ab237712, 1:100 dilutions), rabbit monoclonal [EPR22241] to TIM-3 (ab241332, 1:200 dilutions), rabbit monoclonal [EPR20261] to LAG-3 (ab209236, 1:50 dilutions), and rabbit monoclonal [BLR047F] to TIGIT (ab243903, 1:300 dilutions). And rabbit monoclonal [EPR25200-50] to PD-L2

(ab288298, 1:100 dilutions) was used. 22C3 pharmDx (mouse monoclonal primary anti-PD-L1 antibody, prediluted, clone 22C3, Dako, Carpinteria, CA) on the Autostainer Link 48 according to the manufacturer's instructions. According to the previous study, the pathological assessment of staining was performed using the CPS, and CPS $\geq$1 was considered as positive [32,33]. We used the semi-quantitative scoring method according to a previous study by multiplying the score of staining intensity and the score of positive cells for FTH1 [34]. The low expression was defined as the scores from 0 to 6, and the high expression was defined as the scores from 7 to 12. The Kaplan-Meier (K-M) survival curves by the log-rank test were conducted to analyze the survival differences.

2.11. Statistical analysis

Survival distributions were calculated by using the Kaplan-Meier method (log-rank test). Univariate and multivariate Cox regression models were used to investigate independent prognostic factors associated with OS. The comparisons between PD-L1 expression and clinicopathologic characteristics were performed by chi-squared analysis or Fisher's exact test as appropriate. All statistical analyses were performed using R version 4.1.0. Statistical significance was set at $P < 0.05$.

3. Results

3.1. Identification of B cell marker gene expression profiles

We obtained 64711 cells from 18 treatment-naïve HNSC patients using scRNA-seq data of GSE164690 (Fig. 2a). The screened cells were clustered into 17 clusters by the t-SNE analysis (Fig. 2b). We annotated five cell types, including T cells, B cells, monocyte cells, NK cells, and Epithelial cells, using reference data from the Human Primary Cell Atlas (Fig. 2c). And cells in the 4, 8, and 13 clusters were defined as B cells. Each cluster's top 5 marker genes were specifically expressed (Fig. 2d). Specifically, a total of 145 B cell marker

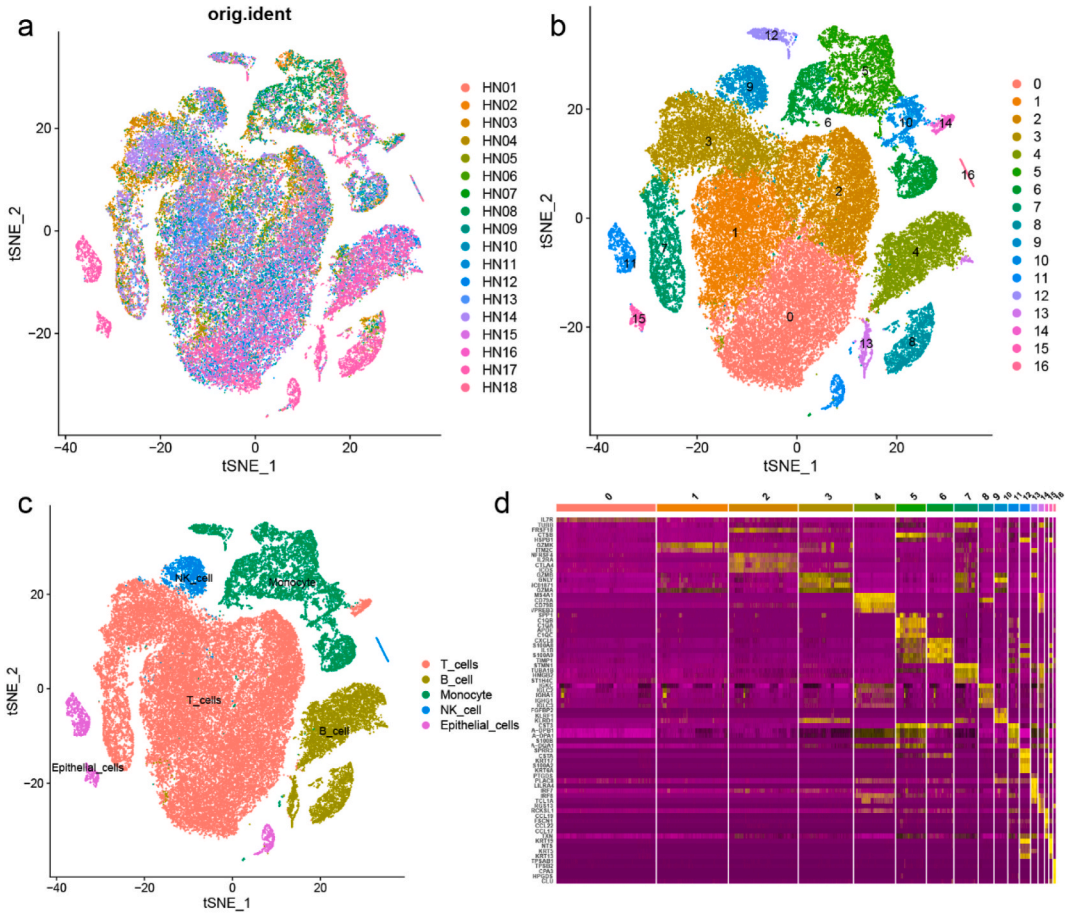

Fig. 2. B cell marker genes were identified by Single-cell RNA-sequencing analysis. (a). T-SNE plot of cells from 18 HNSC samples. (b). T-SNE plot colored by various cell clusters. Each point represents one cell, and the point colors represent the cell samples. (c). T-SNE analysis. Each point's colors represent the specific cell clusters. (d). The expression patterns of the cell type-specific marker genes across the cell clusters. HNSC, head and neck squamous cell carcinoma; T-SNE, The T-distributed Stochastic Neighbor Embedding.

genes were found to be B cell marker genes in HNSC (Table S1).

3.2. Construction of the BCMGS

We first used 145 genes to conduct a univariate Cox regression analysis, and a total of 71 genes were found to be significantly correlated with OS ($P < 0.05$) (Table S2). We further obtained 16 genes with LASSO analysis (Figs. S1a and b, Table S3). After the stepwise multivariable Cox regression analyses, we identified seven genes that were most linked to prognosis (Fig. S1c), and these seven genes were finally used to construct the prognostic model: Risk score = - 0.2323 * expression of FCRLA + 0.2329 * expression of FTH1-0.4335 * expression of LAT - 0.3042 * expression of S100A4 + 0.2714 * expression of TIMP1 - 0.1138 * expression of TNFRSF18 + 0.1382 * expression of TXN (Table S4). The 499 HNSC patients from TCGA were divided into high- and low-risk groups based on the median cut-off value of risk score (0.9882). Two hundred forty-nine patients with a risk score ≥1.2277 were included in the high-risk group, and 250 patients with a risk score ≤0.9521 were included in the low-risk group. The distribution of risk scores and survival status of HNSC patients were displayed in Fig. 3a. The detailed expression levels of these seven genes were shown in the heatmap (Fig. 3b), and the OS of high-risk patients was lower than that of the low-risk patients (Fig. 3c). To assess the performance of the model, we calculated the area under the curve (AUC), and the 2-, 3-, and 5-year AUC were 0.680, 0.675, and 0.625, respectively (Fig. 3d).

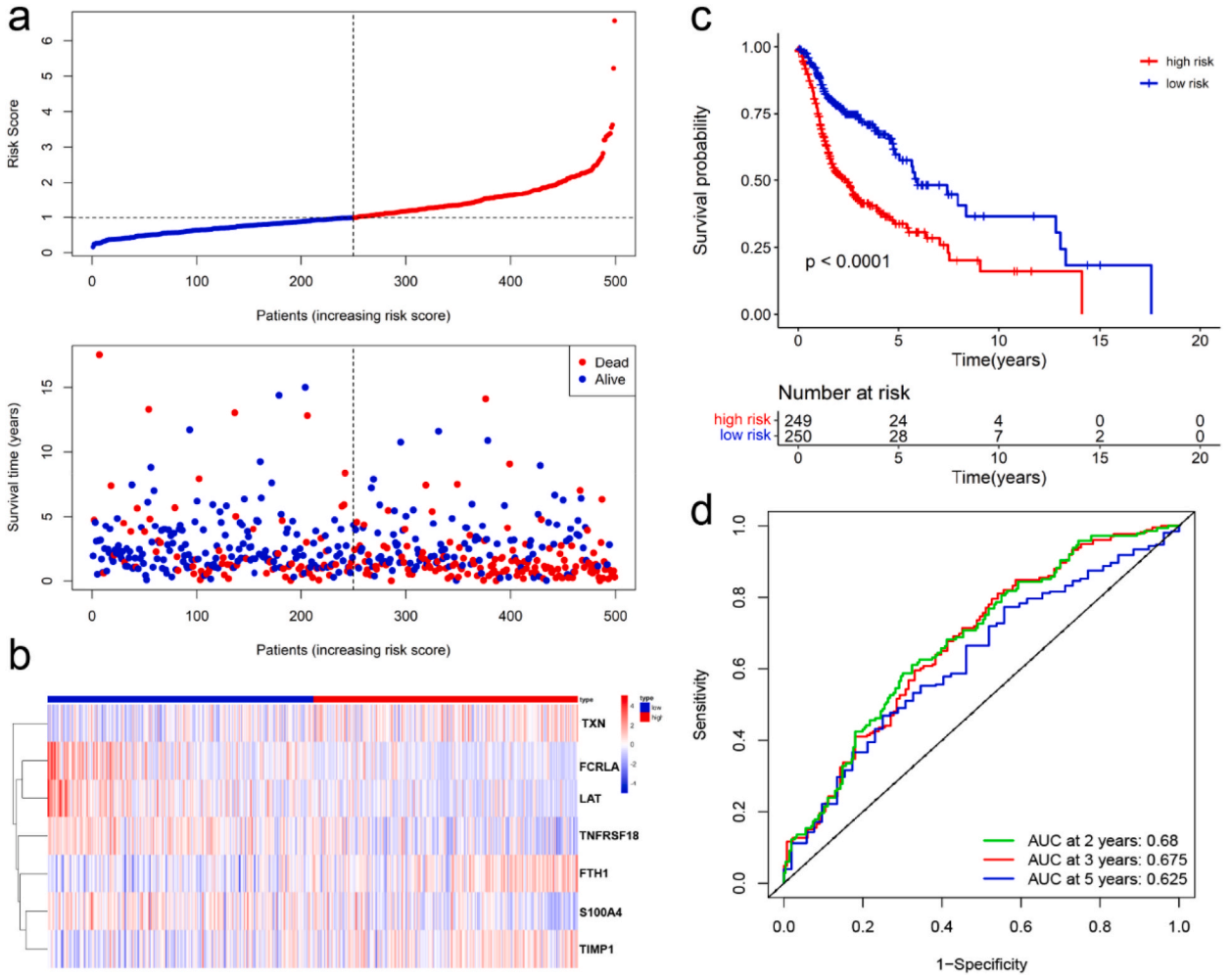

Fig. 3. Construction of the B cell marker genes signature using the TCGA cohort. (a). The risk score distribution and survival status of HNSC patients in the TCGA cohort. High- and low-risk score groups were defined by the median cut-off value. (b). The heatmap exhibited the expression patterns of seven genes in high-risk and low-risk groups. (c). Kaplan-Meier curves of high- and low-risk HNSC patients in TCGA cohort. (d). ROC analysis of the TCGA cohort based on the risk score for predicting the risk of death at 2, 3, and 5 years. TCGA, The Cancer Genome Atlas; HNSC, head and neck squamous cell carcinoma; ROC, receiver operating characteristic.

3.3. Validation of the BCMGS in four other independent cohorts

To validate the predictive power of the BCMGS, we enrolled the GSE41613 (97 samples), GSE42743 (74 samples), and GSE65858 (270 samples), and E-MTAB-8588 (108 samples) expression profile. All the clinical features of these datasets were shown in Table S5. The risk score was calculated by the same formula which was built in the training cohort, and patients in each GEO dataset were divided into two groups by the median cut-off value, excluding the GSE65858 dataset, which used the optimal cut-off value. Similar to the previous training cohort analysis, the Kaplan–Meier analysis showed that the patients in the high-risk group were associated with a worse prognosis ($P < 0.05$; Fig. 4 a-d). The 2-, 3-, and 5-year AUC values were 0.732, 0.713, and 0.685 in the GSE41613 cohort, and 0.663, 0.678, 0.819 in the GSE42743 cohort, and 0.570, 0.571, 0.632 in the GSE65858 cohort, and 0.701, 0.707, 0.695 in the E-MTAB-8588 cohort, respectively (Fig. S2). Our results confirmed that the signature was a risk factor in HNSC (combined HR = 2.134, 95 % CI = 1.651–2.759, meta-analysis $P < 0.001$) (Fig. 4e).

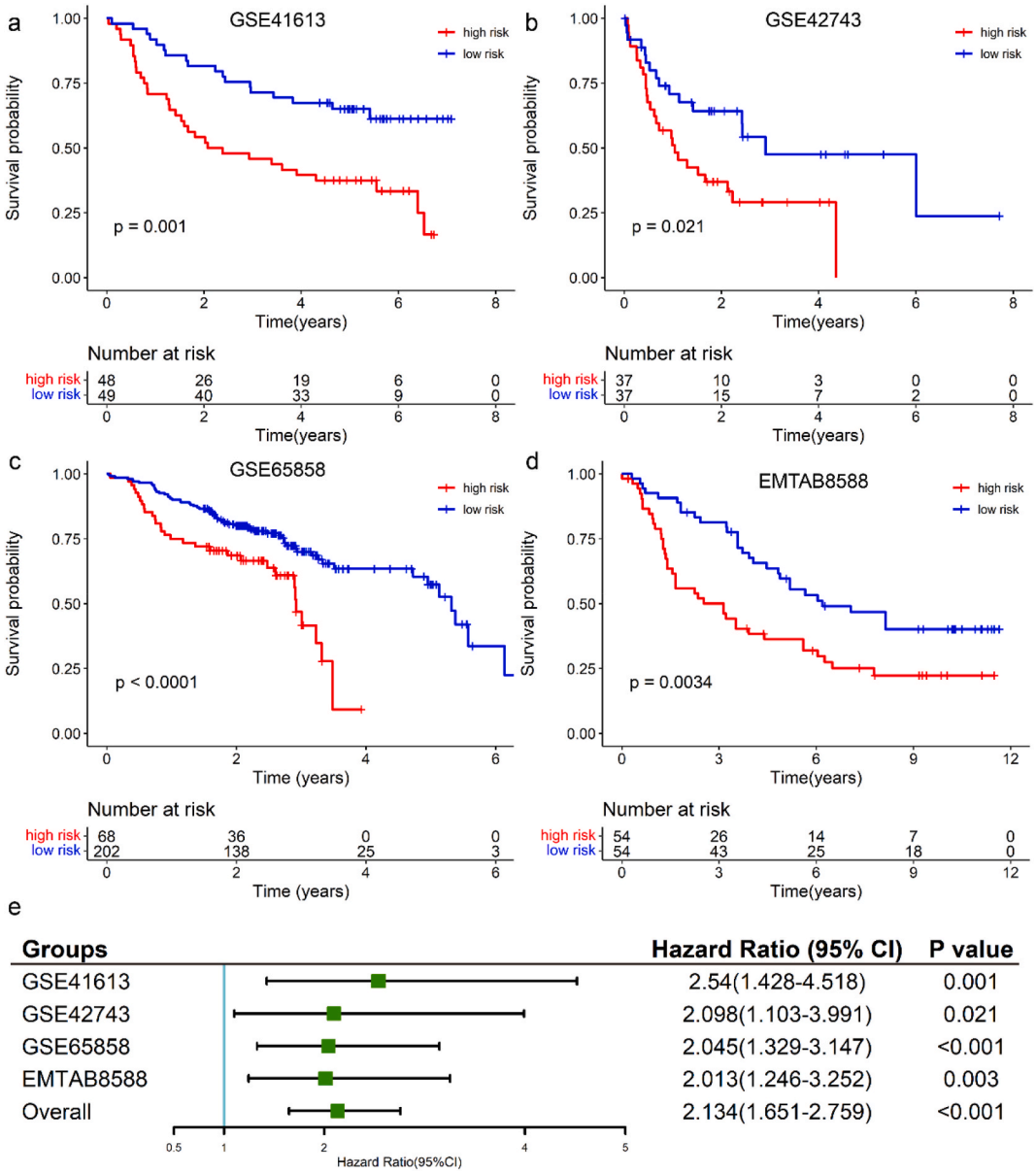

Fig. 4. Validation of the prognostic value of the B cell marker genes signature in four independent datasets. Kaplan-Meier survival analysis of HNSC patients in the GEO cohorts. (a). GSE41613. (b). GSE42743. (c). GSE65858. (d). EMTAB8588 (e). The overall P value was calculated by meta-analysis using the prognostic results of four independent datasets. GEO, Gene Expression Omnibus; HNSC, head and neck squamous cell carcinoma.

3.4. Cox regression analyses and independent risk factors

We used univariate Cox regression analysis and multivariate Cox regression analysis to determine that our BCMGS was independent of other clinical factors and was an independent risk factor for prognosis. The results showed that risk scores (HR, 0.463; 95%CI, 0.331–0.647, $P < 0.001$), T stage (HR, 1.713; 95%CI, 1.185–2.477, $P = 0.004$), lymphatic metastasis (HR, 1.670; 95%CI, 1.197–2.332, $P = 0.003$) and sex (HR, 0.693; 95%CI, 0.497–0.967, $P = 0.031$) were identified as independent predictive factors of prognosis (Table S6). Data stratification analyses were conducted in the training cohort based on the clinicopathological factors. The risk score was still a prognostic factor in the patients stratified by sex, age, grade, T stage, N stage, and stage (Figs. S3 and 4).

3.5. Construction and assessment of a nomogram

Based on the independent predictive factors analyzed by the Cox regression model, including the risk score, tumor stage, nodal stage, and sex, a nomogram for the 2-, 3-, and 5-year OS was constructed to develop a credible method that can predict the OS of HNSC patients (Fig. 5a). 2-, 3-, and 5-year AUC of the nomogram were 0.715, 0.716, 0.614 and the result of the C-index was 0.701 (Fig. 5b). The calibration plots of 2-, 3-, and 5-year also confirmed the prediction reliability of our nomogram (Fig. 5c). The prognostic nomogram had a better discriminative ability to recognize patients at high risk.

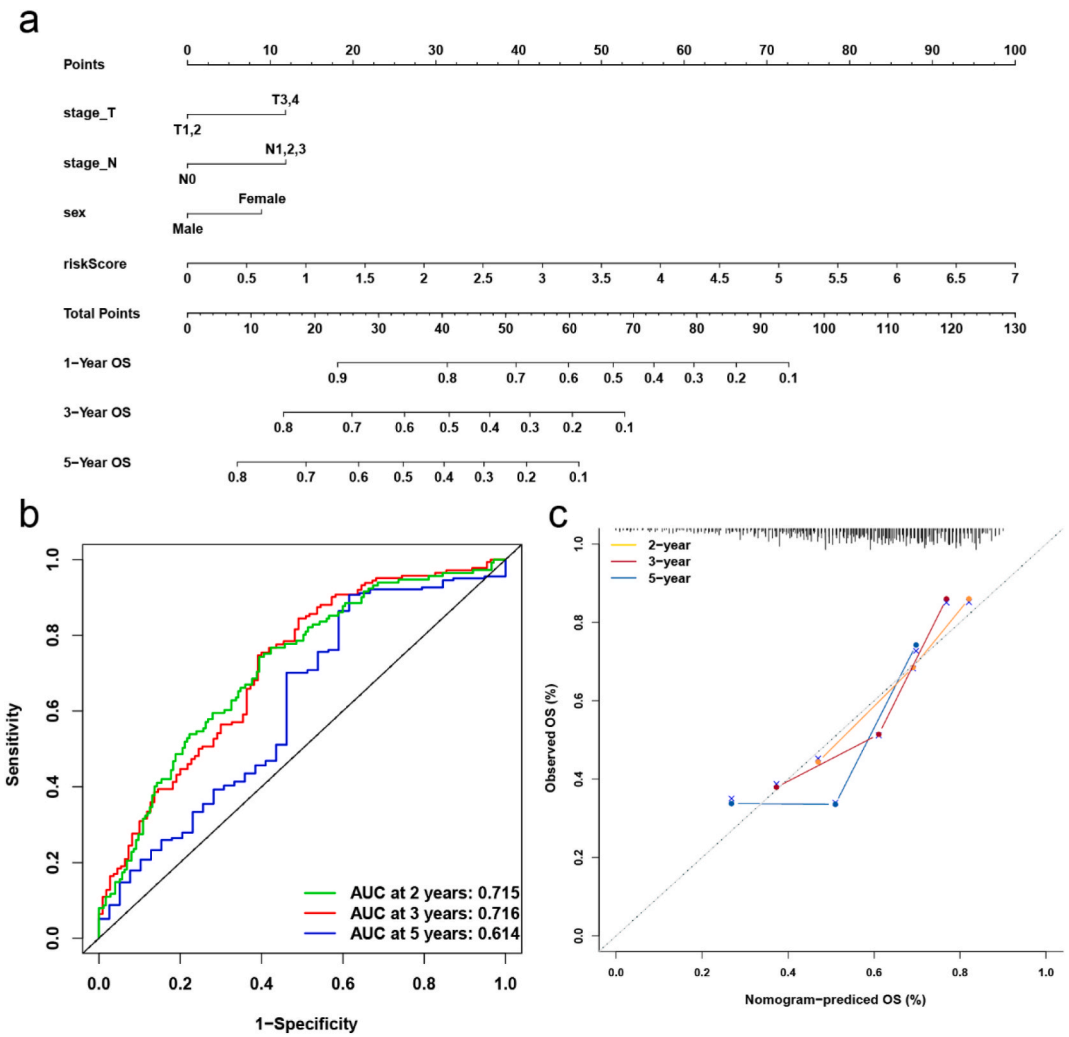

Fig. 5. Nomogram to predict the OS probabilities of HNSC patients in the TCGA cohort. (a). The nomogram. (b). 2-, 3- and 5-year ROC curves. (c). Calibration curves of 2-year, 3-year and 5-year OS. OS, overall survival; HNSC, head and neck squamous cell carcinoma; TCGA, The Cancer Genome Atlas; ROC, receiver operating characteristic.

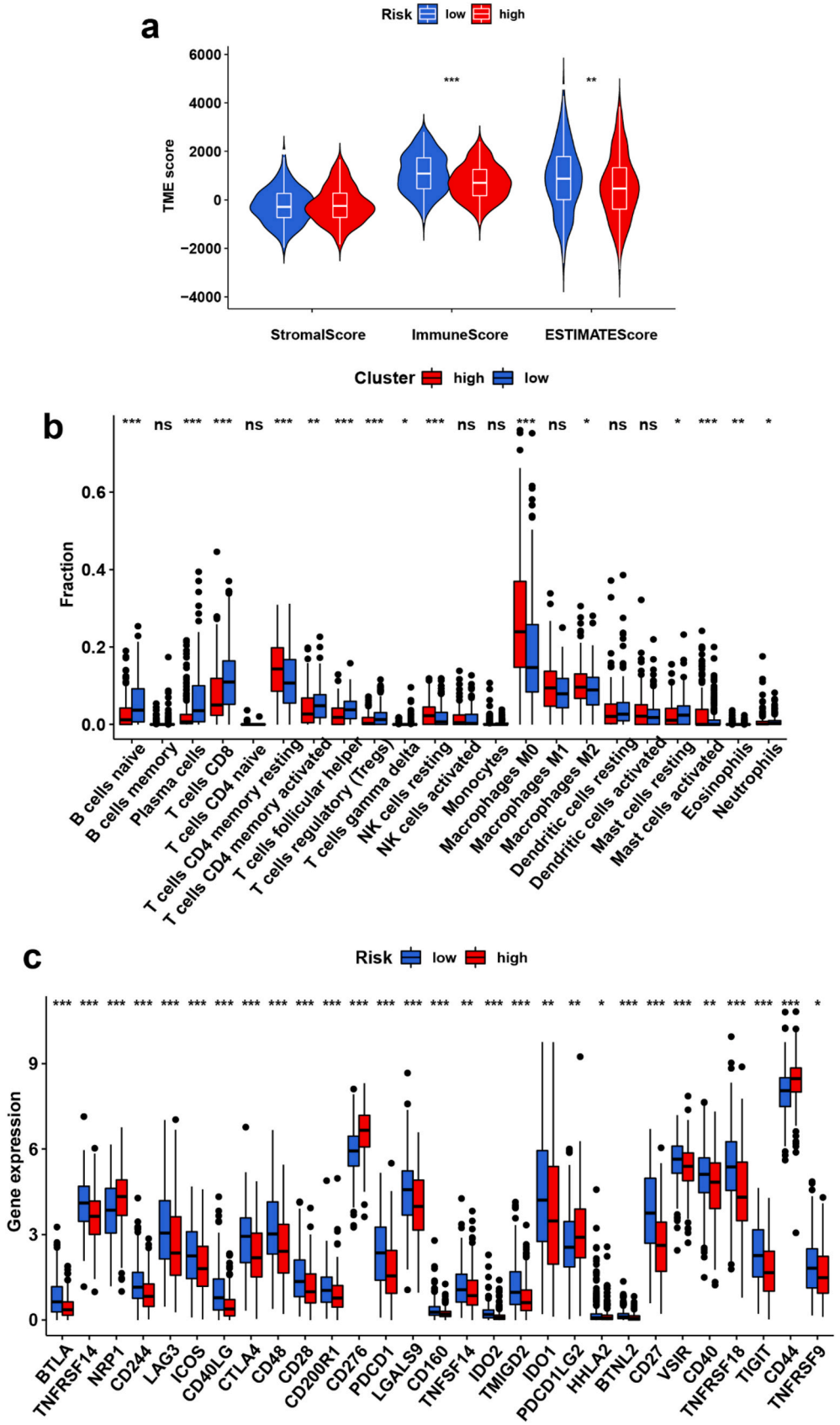

(caption on next page)

Fig. 6. The association between the B cell marker genes signature and the immune cell infiltration in the TME. (a). The relationship between the B cell marker genes signature and immune cell infiltration score in HNSC tumor tissues. (b). 22 immune cells content in the high-risk and low-risk groups. (c). Expression of immune checkpoints in high- and low-risk groups. HNSC, head and neck squamous cell carcinoma; ESTIMATE, The Estimation of Stromal and Immune cells in Malignant Tumor tissues using Expression data.

3.6. Functional enrichment analysis of the BCMGS

The underlying mechanism that the B cell marker genes affected the prognosis of HNSC patients aroused our interest. First, we obtained 2002 DEGs between two risk groups. The detailed information was visualized by the volcano map in Fig. S5a. Then, GO and KEGG enrichment analyses were analyzed. KEGG showed that these genes were primarily involved in neuroactive ligand-receptor interaction, Primary immunodeficiency, nicotine addiction, and cytokine-cytokine receptor interaction (Fig. S5b). GO analysis indicated that these genes were enriched in complement activation (classical pathway), humoral immune response mediated by circulating immunoglobulin, complement activation, immunoglobulin-mediated immune response, and B cell-mediated immunity (Fig. S5c).

3.7. Immune cell infiltration score between high- and low-risk group

The evaluation of immune scores showed a significant difference between high and low-risk groups. More specifically, the high-risk group showed significantly lower immune scores and ESTIMATE scores compared with the low-risk group (Fig. 6a).

3.8. Relationship between immune cell infiltration and the BCMGS

We estimated the presence of 22 immune cell types in the TCGA cohort, and 15 of them showed a significant difference between high- and low-risk groups. We found that increased immune cells infiltration was found in the low-risk group compared with the high-risk group, including naïve B cells, plasma cells, $CD8^+$ T cells, activated $CD4^+$ memory T cells, T cells follicular helper, T cells regulatory (Tregs), T cells gamma delta and resting mast cells (Fig. 6b). However, the high-risk group showed a statistically higher abundance of immune cells, such as resting $CD4^+$ memory T cells, resting NK cells, macrophages M0, macrophages M2, activated mast cells, eosinophils, and neutrophils (Fig. 6b). The immune cell infiltration in high- and low-risk groups was visualized by a violin plot. The associations between 29 immune checkpoints and two risk groups were significantly different among 35 immune checkpoints (Table S7). The high-risk group was associated with high expression of these immune checkpoints except NRP1, CD276, PDCD1LG2, and CD44 (Fig. 6c).

3.9. The difference in immunotherapeutic responsiveness in BCMGS

The immunotherapies used in the selected patients reverse the immunosuppressive microenvironment and attack cancer cells [35]. Previous research demonstrated that TCR and BCR repertoire were correlated with immunotherapy response [36]. In our study, the low-risk group was featured by higher TCR and BCR (Fig. S6), which suggested that low-risk patients may be more sensitive to ICIs.

3.10. Gene expression analysis using GEPIA2

We assessed the expression of seven genes in BCMGS between the normal tissues and tumor tissues. The mRNA expression of FTH1 and TNFRSF18 was significantly highly expressed in tumor tissues compared with normal tissues (Fig. 7). No significant correlation was found in the mRNA expression of FCRLA, LAT, S100A4, TMP1, and TXN between tumor tissues and normal tissues (Fig. 7).

3.11. Validation of the FTH1 expression in HNSC tissues

Considering that FTH1 was a carcinogenic risk factor at the time of model establishment, and it was found that FTH1 was highly expressed in tumor tissues compared with normal tissues when analyzed by GEPIA2. To verify the reliability of the results, we obtained FFPE specimens of 114 HNSC samples. The high expression level of FTH1 in HNSC tissues was significantly correlated with the poor OS ($P = 0.025$, Fig. 8a and b).

3.12. PD-L1 and immune checkpoints expression in HNSC tissues

PD-L1 expression was correlated with the T stage and AJCC stage using the chi-squared test (Table S8). Kaplan-Meier survival analysis demonstrated that high expression of TIM-3 ($P = 0.032$, Fig. 8c and d), LAG-3 ($P = 0.038$, Fig. 8e and f), and PD-1 expression ($P = 0.041$, Fig. 8g and h) were found to be significantly correlated with better OS. However, there was no statistically significant difference between other immune checkpoints in HNSC samples and prognosis, including PD-L1, PD-L2, CTLA-4, and TIGIT (Fig. S7). A multivariate Cox analysis was used to identify the association with OS among prognostic factors. Lymphatic metastasis (HR = 3.53, 95 % CI: 1.14–10.97, $P = 0.029$), LAG-3 positive expression (HR = 0.17, 95 % CI: 0.03–0.91, $P = 0.038$) and FTH1 positive expression (HR = 3.91, 95 % CI: 1.25–12.13, $P = 0.019$) were independent prognostic factors (Table 1).

4. Discussion

With the increasing number of studies with high adoption of High-Throughput Sequencing (HTS) and advances in bioinformatics methods, more and more molecular analyses of cancers were performed, which help to identify the markers to predict the prognosis and immunotherapy response. However, no studies have used BCMGS to investigate tumorigenesis and progression in HNSC. Therefore, in this study, we obtained B cell marker genes in HNSC based on scRNA-seq data and constructed a BCMGS by Cox proportional hazard regression and LASSO regression analysis.

The patients were divided into high- and low-risk groups by risk scores, with significantly different prognoses shown by Kaplan-Meier curves. The signature is an independent prognostic factor verified by multivariate Cox regression analyses. Furthermore, the prognostic prediction power of BCMGS was validated in four other datasets. For better prediction, we successfully used the independent prognostic factors analyzed in previous multivariate Cox regression (risk scores, T stage, and N stage) and constructed a nomogram to estimate the survival probability of HNSC better. The AUC curves and calibration plots demonstrated that it was an accurate and reliable nomogram.

The identified seven genes (FCRLA, FTH1, LAT, S100A4, TMP1, TNFRSF18, and TXN) that established the BCMGS had been previously reported to be associated with tumor formation, development, and prognosis. FCRLA, which acted as an intracellular B cell protein and was the number of the Fc receptor-like (FCRL) family, was the potential tumor-associated antigen of B-cell lymphoma for immunotherapy [37,38]. FTH1 may play a role in promoting tumorigenesis by inducing epithelial-mesenchymal transition, promoting cell proliferation, and inhibiting apoptosis [39–42]. LAT1 has been considered as a molecular target for cancer diagnosis and cancer immunotherapy [43,44]. High LAT expression was correlated to the low OS in Clear cell renal cell carcinoma (ccRCC) samples [45]. S100A4 expression levels are elevated in many tumor types, which enhances cell growth and motility, and eventually increases the possibility of metastatic [46,47]. TMP1, which has been poorly studied in oncology, was identified as a prognosis-related gene in colorectal carcinoma (CRC) [48]. TMP1 also showed a role in in proliferation, invasion and metastasis of OSCC cells in vitro [49]. TNFRSF18 (The glucocorticoid-induced tumor necrosis factor receptor-related gene), also named GITR, played an essential role in conventional T lymphocyte activation as a T cell co-activating molecule and inhibited the proliferation of Treg cells [50]. GITR has

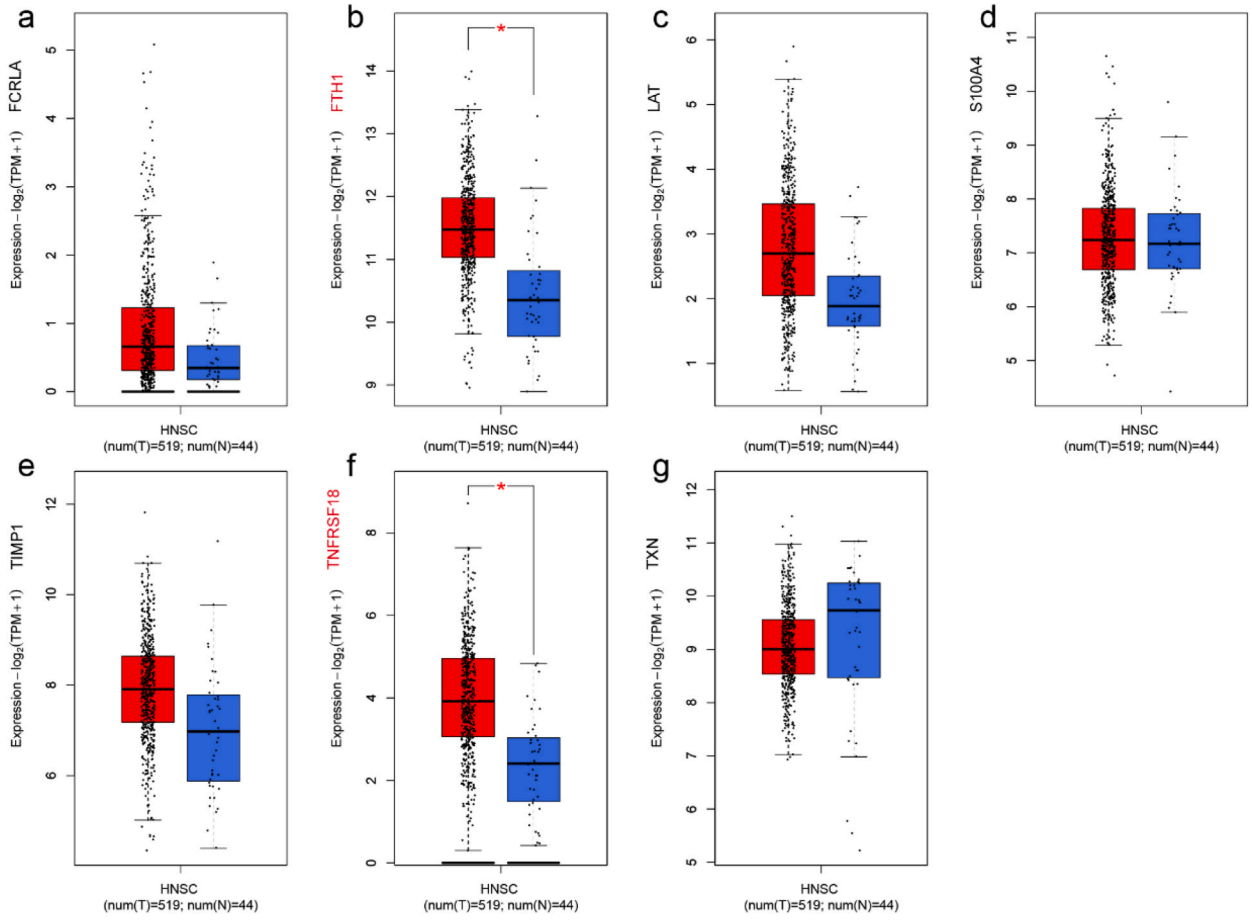

Fig. 7. The expression difference of seven genes in the signature between the tumor tissues from TCGA and the matched normal tissues from TCGA normal and GTEx (Genotype-tissue expression). (a). FCRLA. (b). FTH1. (c). LAT. (d).S100A4. (e). TMP1. (f).TNFRSF18. (g). TXN. $*P < 0.05$.

become an attractive target in cancer immunotherapy singly and as enhancer of other immunotherapy agents [51]. Antibodies targeting GITR were tested in many clinical trials and were well tolerated and safe in patients with solid tumors [52,53]. TXN protein expression was poor prognostic for gastric cancer markers and was overexpressed in gastric cancer tissues [54]. The TXN antioxidant pathway was found to be upregulated in tumor cells which supported cancer cell survival [55].

We performed GO and KEGG analyses of DEGs of high- and low-risk groups to analyze the molecular biological characteristics. GO and KEGG analysis showed that it was mainly enriched in complement activation and humoral immune response. Furthermore, the poor prognosis in the high-risk group may be due to the B cell dysfunction, which participated actively in infiltrating and modulating tumor immunity. The results of functional enrichment analysis inspired us to investigate the mechanism of oncogenesis with the role of TME in HNSC. Our results found that the low-risk group was associated with higher immune scores and ESTIMATE scores. Tumor cells changed the immune microenvironment to an immunosuppressive milieu, which was acknowledged as a hallmark of cancer, to survive and proliferate [56]. It is the primary reason the high-risk group was associated with poor OS. The infiltration of resting $CD4^+$ memory T cells, macrophages M0 and M2 was high in the high-risk group. However, $CD8^+$ T cells, naïve B cells, and activated $CD4^+$ memory T cells showed statistically higher abundance in the low-risk group, which significantly influenced immune status and increased immunity scores in the low-risk group. That's the reason that the overall level of the ESTIMATE score in the high-risk group was significantly lower than the low-risk group in our result.

ICI has been approved as a treatment for HNSC, but only a few patients can benefit from the immunotherapies, so it was vital to identify biomarkers for ICIs response prediction [57,58]. There are many other reasons affecting immunotherapy's efficacy, including TCR and BCR diversity. TCR and BCR repertoire diversity act as not only a good prognostic factor in many tumor types, which shows that higher diversity was associated with a better prognosis, but also a factor to predict potential patients for a better anti-tumor immune response [59–61]. Our findings suggested that patients in the low-risk group may be more sensitive to ICIs treatment. An implication of the relationship between the BMGS and these biomarkers was the possibility that the signature may be used to predict ICIs treatment response.

Immune checkpoints are regulators of the immune system, which can be modulated by tumors to protect themselves from attack by the immune system. Because of the emergence of immune checkpoint blockade (ICB) in immunotherapy, it has experienced radical clinical progress in cancer therapy [62]. PD-1, TIM-3, LAG-3, and CTLA-4 are inhibitory receptors that induce a negative signal to T cells. However, high expression of ICs associated with good prognosis in some tumors reflects an increased activated immune response [63]. Hence, the correlations between prognosis and expression of immune checkpoints in various types of cancer remain controversial [64–68]. In our study, the expression of TIM-3, LAG-3, and PD-1 is positively correlated and associated with better OS in HNSC patients.

According to our understanding, this is the first bioinformatics analysis to investigate the signature using B cell marker genes in HNSC. The findings could help to predict the prognosis and the response to immunotherapy. Nevertheless, several limitations of this study need to be acknowledged. First, all the patients were enrolled from TCGA, GEO, and ArrayExpress databases, which were derived from retrospective studies, and prospective study of vitro or vivo experiments should be carried out. Second, the other clinical factors, such as the M staging and the location of distant metastasis, were not available in the public dataset, which made it difficult to incorporate more variables in the nomogram. Third, it was not sufficient for ICIs response prediction to use a single characteristic to establish the signature, and B cell marker genes were only one aspect to influence the progression of HNSC. Fourth, the methods of PCA have some limitations, including linearity assumption, sensitivity to outliers, loss of feature interpretability, and the need for judicious

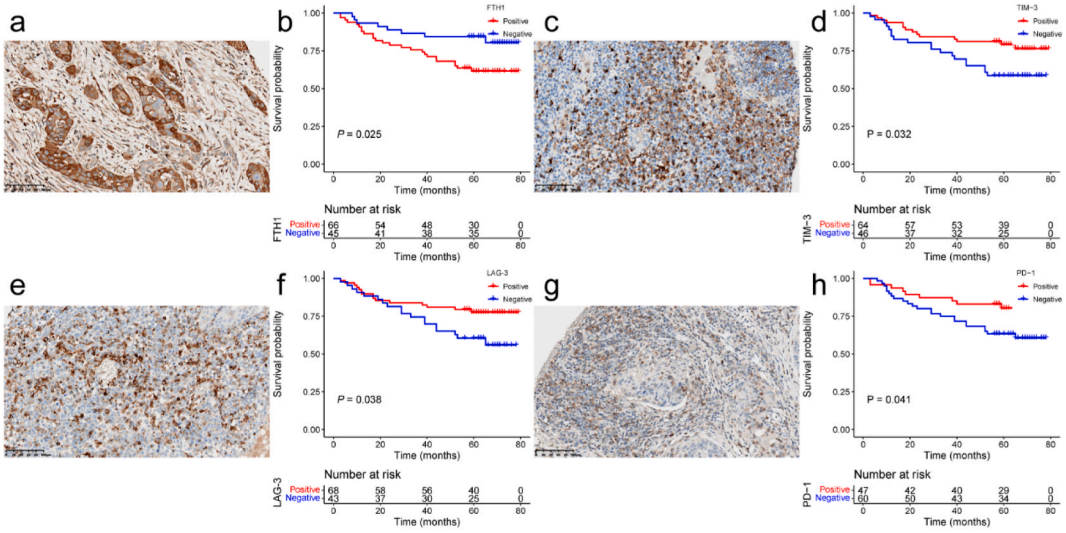

Fig. 8. Representative IHC images and Kaplan-Meier curves. High expression of FTH1 (a), TIM-3 (c), LAG-3 (e), PD-1 (g) in HNSC. Kaplan-Meier analysis of the association between OS and FTH1 expression (b), TIM-3 expression (d), LAG-3 expression (f), PD-1 expression (h). All pictures are taken at × 400 magnification. HNSC, head and neck squamous cell carcinoma; IHC, immunohistochemistry.

Table 1
Univariate and multivariate Cox analysis for Overall survival in patients with head and neck squamous cell carcinomas (N = 114).

Variables	Overall survival			
	Univariate		Multivariate	
	HR(95%CI)	*P*	HR(95%CI)	*P*
Male	0.74 (0.31–1.79)	0.503		
Age≥60	1.27 (0.62–2.62)	0.515		
T3&T4	1.19 (0.60–2.36)	0.612		
Lymphatic metastasis	3.09 (1.53–6.22)	**0.002**	3.53 (1.14–10.97)	**0.029**
Stage III&IV	2.06 (0.93–4.57)	0.076		
Lymphovascular invasion	3.51 (1.51–8.13)	**0.003**	2.30 (0.80–6.61)	0.122
Perineural invasion	2.60 (1.15–5.91)	**0.022**	2.37 (0.94–5.98)	0.068
Smoking	0.89 (0.41–1.92)	0.765		
Drinking	1.23 (0.61–2.48)	0.559		
PD-L1 positive	0.65 (0.30–1.39)	0.267		
TIM-3 positive	0.48 (0.24–0.95)	**0.036**	1.22 (0.39–3.77)	0.736
LAG-3 positive	0.49 (0.25–0.98)	**0.043**	0.17 (0.03–0.91)	**0.038**
CTLA-4 positive	0.62 (0.30–1.27)	0.192		
TIGIT positive	1.26 (0.62–2.55)	0.528		
PD-1 positive	0.46 (0.21–0.99)	**0.046**	0.95 (0.22–4.12)	0.946
PD-L2 positive	1.13 (0.55–2.33)	0.739		
FTH1 positive	2.42 (1.09–5.37)	**0.030**	3.91 (1.25–12.13)	**0.019**

component selection. PCA aims to reduce dimensionality by retaining the most significant information, but there is always some loss of information when reducing the number of dimensions.

5. Conclusions

In this study, we selected B cell marker genes of HNSC using scRNA-seq data and identified high- and low-risk subgroups based on the BCMGS through LASSO and Cox regression analysis. Four independent datasets well demonstrated its prediction efficiency. The survival and immune status of the two subgroups were significantly different. This study found the BCMGS as a possible response indicator to predict the prognosis and tumor immunotherapy and provided a new perspective for future research on the treatment of HNSC.

Funding

This research was funded by Non-profit Central Research Institute Fund of Chinese Academy of Medical Science, Grant Number: 2019-RC-HL-004; Beijing Hope Run Special Fund of Cancer Foundation of China, Grant Number: No. LC2020A19. Sanming Project of Medicine in Shenzhen, Grant Number: No. SZSM201911006.

Ethics statement

The Ethics Committee of Cancer Hospital, Chinese Academy of Medical Sciences approved our study. The ethics approval number is NCC2020C-471.

Data availability statement

Data associated with the study has not been deposited into a publicly available repository. Data will be made available on request.

CRediT authorship contribution statement

Dilinaer Wusiman: Writing - review & editing, Writing - original draft, Software, Formal analysis, Data curation. **Wenbin Li:** Writing - review & editing, Writing - original draft, Validation, Supervision, Resources, Conceptualization. **Lei Guo:** Writing - review & editing, Writing - original draft, Validation, Supervision, Resources, Methodology, Investigation, Data curation. **Zehao Huang:** Writing - review & editing, Writing - original draft, Validation, Software, Resources, Methodology. **Yi Zhang:** Writing - review & editing, Writing - original draft, Visualization, Validation, Methodology, Investigation. **Xiwei Zhang:** Writing - review & editing, Writing - original draft, Visualization, Validation, Methodology, Data curation. **Xiaohui Zhao:** Writing - review & editing, Writing - original draft, Software, Resources, Methodology, Investigation. **Lin Li:** Writing - review & editing, Writing - original draft, Visualization, Resources, Data curation. **Zhaohong An:** Writing - review & editing, Writing - original draft, Visualization, Validation, Software. **Zhengjiang Li:** Writing - review & editing, Writing - original draft, Supervision, Resources, Project administration, Conceptualization. **Jianming Ying:** Writing - review & editing, Writing - original draft, Supervision, Project administration, Conceptualization. **Changming An:** Writing - review & editing, Writing - original draft, Supervision, Resources, Project

administration, Investigation, Funding acquisition, Conceptualization.

Declaration of competing interest

The authors declare that they have no known competing financial interests or personal relationships that could have appeared to influence the work reported in this paper.

Acknowledgments

All authors would like to thank the specimen donors and research groups for the TCGA, GSE41613, GSE42743, GSE65858, and E-MTAB-8588 which provided data for this article.

Appendix A. Supplementary data

Supplementary data to this article can be found online at https://doi.org/10.1016/j.heliyon.2023.e22656.

References

[1] H. Sung, et al., Global cancer statistics 2020: GLOBOCAN estimates of incidence and mortality worldwide for 36 cancers in 185 countries, CA Cancer J Clin 71 (3) (2021) 209–249.
[2] M.L. Hedberg, J.R. Grandis, The molecular pathogenesis of head and neck cancer, in: The Molecular Basis of Cancer, fourth ed., 2015, pp. 491–498.e2.
[3] L.Q.M. Chow, Head, Neck Cancer, N. Engl. J. Med. 382 (1) (2020) 60–72.
[4] M.B. Howren, et al., Problem alcohol use among rural head and neck cancer patients at diagnosis: associations with health-related quality of life, Psycho Oncol. 30 (5) (2021) 708–715.
[5] A.R. Jethwa, S.S. Khariwala, Tobacco-related carcinogenesis in head and neck cancer, Cancer Metastasis Rev. 36 (3) (2017) 411–423.
[6] J.C. Nogues, et al., Human papillomavirus-associated head and neck cancer, J. Am. Board Fam. Med. 34 (4) (2021) 832–837.
[7] H. Mehanna, et al., Prevalence of human papillomavirus in oropharyngeal and nonoropharyngeal head and neck cancer–systematic review and meta-analysis of trends by time and region, Head Neck 35 (5) (2013) 747–755.
[8] B. Burtness, et al., Pembrolizumab alone or with chemotherapy versus cetuximab with chemotherapy for recurrent or metastatic squamous cell carcinoma of the head and neck (KEYNOTE-048): a randomised, open-label, phase 3 study, Lancet 394 (10212) (2019) 1915–1928.
[9] X. Wu, et al., Application of PD-1 blockade in cancer immunotherapy, Comput. Struct. Biotechnol. J. 17 (2019) 661–674.
[10] A. Haque, et al., A practical guide to single-cell RNA-sequencing for biomedical research and clinical applications, Genome Med. 9 (1) (2017) 75.
[11] L. Zhu, et al., A UNIFIED statistical framework for single cell and bulk RNA sequencing data, Ann. Appl. Stat. 12 (1) (2018) 609–632.
[12] D.S. Thommen, T.N. Schumacher, T cell dysfunction in cancer, Cancer Cell 33 (4) (2018) 547–562.
[13] M. Horii, T. Matsushita, Regulatory B cells and T cell regulation in cancer, J. Mol. Biol. 433 (1) (2021), 166685.
[14] X. Ren, et al., Insights gained from single-cell analysis of immune cells in the tumor microenvironment, Annu. Rev. Immunol. 39 (2021) 583–609.
[15] Q. Li, et al., Adoptive transfer of tumor reactive B cells confers host T-cell immunity and tumor regression, Clin. Cancer Res. 17 (15) (2011) 4987–4995.
[16] R. Cabrita, et al., Tertiary lymphoid structures improve immunotherapy and survival in melanoma, Nature 577 (7791) (2020) 561–565.
[17] B.A. Helmink, et al., B cells and tertiary lymphoid structures promote immunotherapy response, Nature 577 (7791) (2020) 549–555.
[18] F. Petitprez, et al., B cells are associated with survival and immunotherapy response in sarcoma, Nature 577 (7791) (2020) 556–560.
[19] Y. Qin, et al., Tumor-infiltrating B cells as a favorable prognostic biomarker in breast cancer: a systematic review and meta-analysis, Cancer Cell Int. 21 (1) (2021) 310.
[20] Z.W. Hu, et al., Ferroptosis driver SOCS1 and suppressor FTH1 independently correlate with M1 and M2 macrophage infiltration in head and neck squamous cell carcinoma, Front. Cell Dev. Biol. 9 (2021), 727762.
[21] Z.W. Hu, et al., Comprehensive analysis of ferritin subunits expression and positive correlations with tumor-associated macrophages and T regulatory cells infiltration in most solid tumors, Aging (Albany NY) 13 (8) (2021) 11491–11506.
[22] M.J. Goldman, et al., Visualizing and interpreting cancer genomics data via the Xena platform, Nat. Biotechnol. 38 (6) (2020) 675–678.
[23] G.P. Wagner, K. Kin, V.J. Lynch, Measurement of mRNA abundance using RNA-seq data: RPKM measure is inconsistent among samples, Theory Biosci 131 (4) (2012) 281–285.
[24] P. Lohavanichbutr, et al., A 13-gene signature prognostic of HPV-negative OSCC: discovery and external validation, Clin. Cancer Res. 19 (5) (2013) 1197–1203.
[25] J. Novotný, et al., Analysis of HPV-positive and HPV-negative head and neck squamous cell carcinomas and paired normal mucosae reveals cyclin D1 deregulation and compensatory effect of cyclin D2, Cancers 12 (4) (2020).
[26] C.H.L. Kürten, et al., Investigating immune and non-immune cell interactions in head and neck tumors by single-cell RNA sequencing, Nat. Commun. 12 (1) (2021) 7338.
[27] N.A. Mabbott, et al., An expression atlas of human primary cells: inference of gene function from coexpression networks, BMC Genom. 14 (2013) 632.
[28] N. Simon, et al., Regularization paths for cox's proportional hazards model via coordinate descent, J Stat Softw 39 (5) (2011) 1–13.
[29] K. Yoshihara, et al., Inferring tumour purity and stromal and immune cell admixture from expression data, Nat. Commun. 4 (2013) 2612.
[30] J.I. Kawada, et al., Immune cell infiltration landscapes in pediatric acute myocarditis analyzed by CIBERSORT, J. Cardiol. 77 (2) (2021) 174–178.
[31] V. Thorsson, et al., The immune landscape of cancer, Immunity 48 (4) (2018) 812–830.e14.
[32] D. Wusiman, et al., The clinicopathological significance of PD-L1 expression assessed by the combined positive score (CPS) in head and neck squamous cell carcinoma, Pathol. Res. Pract. 236 (2022), 153934.
[33] X. Shi, et al., Immune Co-inhibitory receptors PD-1, CTLA-4, TIM-3, LAG-3, and TIGIT in medullary thyroid cancers: a large cohort study, J. Clin. Endocrinol. Metab. 106 (1) (2021) 120–132.
[34] P. Song, et al., Pan-cancer analysis combined with experiments explores the oncogenic role of spindle apparatus coiled-coil protein 1 (SPDL1), Cancer Cell Int. 22 (1) (2022) 49.
[35] W. Zhang, Z. Zhao, F. Li, Natural killer cell dysfunction in cancer and new strategies to utilize NK cell potential for cancer immunotherapy, Mol. Immunol. 144 (2022) 58–70.
[36] D. Zeng, et al., Tumor microenvironment characterization in gastric cancer identifies prognostic and immunotherapeutically relevant gene signatures, Cancer Immunol. Res. 7 (5) (2019) 737–750.
[37] T. Inozume, et al., Dendritic cells transduced with autoantigen FCRLA induce cytotoxic lymphocytes and vaccinate against murine B-cell lymphoma, J. Invest. Dermatol. 127 (12) (2007) 2818–2822.

[38] T. Santiago, et al., FCRLA is a resident endoplasmic reticulum protein that associates with intracellular Igs, IgM, IgG and IgA, Int. Immunol. 23 (1) (2011) 43–53.
[39] S.I. Shpyleva, et al., Role of ferritin alterations in human breast cancer cells, Breast Cancer Res. Treat. 126 (1) (2011) 63–71.
[40] F. Liu, et al., FTH1 binds to Daxx and inhibits Daxx-mediated cell apoptosis, Mol. Biol. Rep. 39 (2) (2012) 873–879.
[41] D.C. Yang, et al., Antisense ferritin oligonucleotides inhibit growth and induce apoptosis in human breast carcinoma cells, Anticancer Res. 22 (3) (2002) 1513–1524.
[42] A. Ali, et al., Ferritin heavy chain (FTH1) exerts significant antigrowth effects in breast cancer cells by inhibiting the expression of c-MYC, FEBS Open Bio 11 (11) (2021) 3101–3114.
[43] K. Hayashi, N. Anzai, L-type amino acid transporter 1 as a target for inflammatory disease and cancer immunotherapy, J. Pharmacol. Sci. 148 (1) (2022) 31–40.
[44] Y. Kanai, Amino acid transporter LAT1 (SLC7A5) as a molecular target for cancer diagnosis and therapeutics, Pharmacol. Ther. 230 (2022), 107964.
[45] J. Wang, et al., LAT, HOXD3 and NFE2L3 identified as novel DNA methylation-driven genes and prognostic markers in human clear cell renal cell carcinoma by integrative bioinformatics approaches, J. Cancer 10 (26) (2019) 6726–6737.
[46] A.R. Bresnick, D.J. Weber, D.B. Zimmer, S100 proteins in cancer, Nat. Rev. Cancer 15 (2) (2015) 96–109.
[47] Z. Ling, R. Li, Clinicopathological and prognostic value of S100A4 expression in gastric cancer: a meta-analysis, Int. J. Biol. Markers 29 (2) (2014) e99–e111.
[48] J. Yang, et al., Integrated Analysis of Gene Expression and Metabolite Data Reveals Candidate Molecular Markers in Colorectal Carcinoma, Cancer Biother Radiopharm, 2020.
[49] T. Takenawa, et al., Silencing of Tropomyosin 1 suppresses the proliferation, invasion and metastasis of oral squamous cell carcinoma in vitro, Journal of Oral and Maxillofacial Surgery, Medicine, and Pathology 35 (3) (2023) 282–287.
[50] D.L. Clouthier, T.H. Watts, Cell-specific and context-dependent effects of GITR in cancer, autoimmunity, and infection, Cytokine Growth Factor Rev. 25 (2) (2014) 91–106.
[51] L. Kraehenbuehl, et al., Enhancing immunotherapy in cancer by targeting emerging immunomodulatory pathways, Nat. Rev. Clin. Oncol. 19 (1) (2022) 37–50.
[52] A.S. Balmanoukian, et al., Safety and clinical activity of MEDI1873, a novel GITR agonist, in advanced solid tumors, Clin. Cancer Res. 26 (23) (2020) 6196–6203.
[53] S.A. Piha-Paul, et al., First-in-human phase I/Ib open-label dose-escalation study of GWN323 (anti-GITR) as a single agent and in combination with spartalizumab (anti-PD-1) in patients with advanced solid tumors and lymphomas, J Immunother Cancer 9 (8) (2021).
[54] J.Y. Lim, et al., Thioredoxin and thioredoxin-interacting protein as prognostic markers for gastric cancer recurrence, World J. Gastroenterol. 18 (39) (2012) 5581–5588.
[55] Isaac S. Harris, et al., Glutathione and thioredoxin antioxidant pathways synergize to drive cancer initiation and progression, Cancer Cell 27 (2) (2015) 211–222.
[56] J.P. Bates, et al., Mechanisms of immune evasion in breast cancer, BMC Cancer 18 (1) (2018) 556.
[57] Q. Chen, T. Li, W. Yue, Drug response to PD-1/PD-L1 blockade: based on biomarkers, OncoTargets Ther. 11 (2018) 4673–4683.
[58] M.J. Duffy, J. Crown, Biomarkers for predicting response to immunotherapy with immune checkpoint inhibitors in cancer patients, Clin. Chem. 65 (10) (2019) 1228–1238.
[59] J.H. Cui, et al., TCR repertoire as a novel indicator for immune monitoring and prognosis assessment of patients with cervical cancer, Front. Immunol. 9 (2018) 2729.
[60] K.R. Lin, et al., T cell receptor repertoire profiling predicts the prognosis of HBV-associated hepatocellular carcinoma, Cancer Med. 7 (8) (2018) 3755–3762.
[61] C. Keane, et al., The T-cell receptor repertoire influences the tumor microenvironment and is associated with survival in aggressive B-cell lymphoma, Clin. Cancer Res. 23 (7) (2017) 1820–1828.
[62] C. Robert, A decade of immune-checkpoint inhibitors in cancer therapy, Nat. Commun. 11 (1) (2020) 3801.
[63] L. Tu, et al., Assessment of the expression of the immune checkpoint molecules PD-1, CTLA4, TIM-3 and LAG-3 across different cancers in relation to treatment response, tumor-infiltrating immune cells and survival, Int. J. Cancer 147 (2) (2020) 423–439.
[64] N. Sauer, et al., LAG-3 as a potent target for novel anticancer therapies of a wide range of tumors, Int. J. Mol. Sci. 23 (17) (2022).
[65] A. Matikas, et al., PD-1 protein and gene expression as prognostic factors in early breast cancer, ESMO Open 5 (6) (2020), e001032.
[66] S. Jiang, et al., Prognostic value of PD-1, PD-L1 and PD-L2 deserves attention in head and neck cancer, Front. Immunol. 13 (2022), 988416.
[67] Y. Liu, et al., The landscape of immune checkpoints expression in non-small cell lung cancer: a narrative review, Transl. Lung Cancer Res. 10 (2) (2021) 1029–1038.
[68] Y. Park, et al., Expression of the immune checkpoint receptors PD-1, LAG3, and TIM3 in the immune context of stage II and III gastric cancer by using single and chromogenic multiplex immunohistochemistry, OncoImmunology 10 (1) (2021), 1954761.